Available online at www.sciencedirect.com
SCIENCE DIRECT
International Journal of Mass Spectrometry 251 (2006) 73–81
International Journal of Mass Spectrometry
www.elsevier.com/locate/ijms

A novel principle for an ion mirror design in time-of-flight mass spectrometry

S. Scherer [a,*], K. Altwegg [a], H. Balsiger [a], J. Fischer [a], A. Jäckel [a], A. Korth [b], M. Mildner [a,1], D. Piazza [a], H. Reme [c], P. Wurz [a]

[a] *University of Bern, Physics Institute, Space Research and Planetary Science Division, Sidlerstrasse 5, CH-3012 Bern, Switzerland*
[b] *Max Planck Institute für Aeronomie, D-37191 Katlenburg-Lindau, Germany*
[c] *Centre d'Etude Spatiale des Rayonnements, F-31029 Toulouse, France*

Received 19 October 2005; received in revised form 9 January 2006; accepted 10 January 2006
Available online 17 February 2006

Abstract

A novel design for a gridless two-stage ion mirror, or reflectron, for time-of-flight mass spectrometry (TOFMS) will be presented. The development of this novel design was driven by the stringent engineering requirements for the ion mirror's utilization by the reflectron time-of-flight (RTOF) sensor in the Rosetta orbiter spectrometer for ion and neutral analysis (ROSINA) instrument package of the Rosetta cometary mission launched by the European Space Agency in March 2004.

The reflectron consists of ceramic and titanium alloy components joined by brazing and welding processes. The device serves as both the mechanical structure and as an ultra-high-vacuum (UHV) enclosure for the TOFMS system. The electrostatic fields of the reflectron are generated along two individually adjustable sections of a resistor helix applied to the inner surface of a ceramic cylinder. This design allows for increased homogeneity of the electrostatic fields, and minimizes fringe fields close to the cylindrical boundary of the reflectron structure. Thus, the usable inner diameter of ion flight path for a given outer diameter is maximized; a feature required by spacecraft constraints. An additional electrostatic lens in front of the reflectron allows the geometrical alteration of the shape of the ion beam, and its direction with regard to the ion optical axis. This makes it possible to switch the operation of the TOFMS system between a single-reflection and a triple-reflection mode, the latter using an additional ion mirror. Typically, mass resolutions of up to 5000 at full width at half maximum (FWHM) have been achieved in the triple-reflection mode for an overall sensor dimension of 1 m. Experimental results in the single-reflection mode and in the triple-reflection mode will be presented. Environmental constraints for space applications will also be discussed.

Keywords: Time-of-flight mass spectrometry; Ion mirror; Reflectron; Multiple reflection

1. Introduction

We describe a novel design of the ion mirror (a reflectron) of the RTOF (reflectron time-of-flight) sensor. No commercially available device satisfied the stringent engineering requirements needed for the ROSINA instrument package on board the Rosetta cometary mission. Using the presented design, the RTOF sensor was successfully launched by the European Space Agency (ESA) in March 2004.

In the simplest form of a time-of-flight mass spectrometer (TOFMS) an ion packet is formed in an ion source, accelerated, and recorded on a detector at the end of a field-free drift path. Such a linear time-of-flight mass spectrometer, was presented by Wiley and McLaren [1] using an electron impact ion source with two-stage ion acceleration. This type of instrument, although very successful at its time, has limitations in mass resolution, which rarely exceed 1000.

Several modifications of the basic principle have been subsequently described, with the use of a reflectron being the most successful. Using a reflectron in the TOFMS will cause the ions to reverse their direction of motion at the end of the field-free drift path, thus, doubling the flight path while preserving the overall

* Corresponding author at: University of Michigan, Department for Atmospheric, Oceanic and Space Sciences, Space Physics Research Laboratory, 2455 Hayward, Ann Arbor, MI 48109, USA.
Tel.: +1 734 647 3380; fax: +1 734 615 9723.
E-mail address: sscherer@umich.edu (S. Scherer).
[1] COMET AG, Business Unit X-Ray, Herrengasse 10, CH-3175 Flamatt, Switzerland.

1387-3806/$ – see front matter © 2006 Elsevier B.V. All rights reserved.
doi:10.1016/j.ijms.2006.01.025

geometrical dimensions of the TOFMS system. The reflectron was introduced in 1972 by Karataev et al. [2] and Mamyrin et al. [3]. Two electrostatic fields, one retarding and the other repelling, accomplish ion reflection. The retarding electrostatic field will decelerate the incoming ions and accelerate the outgoing ions, respectively, whereas the repelling electrostatic field actually reverses the ion's flight direction. The electrostatic fields in these reflectrons are established using fine-meshed grids to define the individual fields in the retarding and repelling regions. Having two independently adjustable electrostatic fields allows for a second-order time focusing of the ion packet by the reflectron, resulting in high mass resolution. This design allows a fully analytical treatment to determine the second-order focusing condition [3,4]. From the analytical solution it follows that in a two-stage reflectron the ions have to lose at least two-thirds of their kinetic energy in the retarding field of the reflectron, and the remaining energy in the repelling region. Mass resolution as high as 35,000 have been reported by Bergmann et al. [5].

The ion packets from a pulsed ion source have an initial energy distribution of about ±10% around the nominal ion energy. Ions with higher energy will be faster on the field-free drift path (negative TOF dispersion) but will penetrate deeper into the repelling field before returning (positive TOF dispersion). Consequently, ions with higher energy have a longer time of flight through the reflectron than ions with lower energy. If this longer time of flight in the reflectron compensates for the shorter time of flight in the field-free drift path, ions with an initial energy distribution and the same mass-over-charge ratio will reach the detector entrance plane simultaneously. Typically, an ion energy spread of ±10% around the reference energy can be accommodated in a second-order focusing reflectron design [4,19]. The contributions of third- or higher-order terms, due to the energy distribution of the ions in a second-order focusing reflectron, are more than an order of magnitude smaller than the typical time spread contributions originating from the ion sources.

Using grids results in transmission losses due to the finite grid transparency. This does not include effects caused by the field distortions of the individual grid cells. Experimental evidence shows that the ion-optical transmission of a two-stage reflectron with grids is around 10%, as a result of the defocusing lenses of the individual grid cells. Obviously, several groups have sought to design an ion mirror without grids to improve the sensitivity of the instrument by a factor of 10. Gridless ion mirrors were described, for example, by Walter et al. [6] in 1986, by Grix et al. [7] in 1988, by Wurz in 1990 [4], and by Kutscher et al. [8] in 1991. The reported mass resolutions range from 10,000 [6] to 28,000 [7]. In gridless reflectrons the electrostatic field continuously changes in the interface region between the retarding and repelling fields, and the electric field extends out from the retarding field region into the field-free drift path. An additional advantage of the gridless reflectron results from the inhomogeneous electrical fields, which have geometrical focusing properties, further enhancing the sensitivity of the system [4,9] compared to a conventional reflectron with grids. A theoretical treatment of a gridless reflectron with inhomogeneous electrical fields was given by Wurz [4] in 1990, Bergmann et al. [5,10] in 1990, and Kutscher et al. [8] in 1991. Prototypes of gridless ion reflectrons were described by Grix et al. [7] in 1988 and Kutscher et al. [8] in 1991.

There are a several reports in the literature of laboratory TOFMS systems performing multiple reflections using various ion-optical geometries. For compact TOFMS systems using *Z*-shaped trajectories, the ions pass each reflectron only once. With this approach mass resolutions between 1000 and 3000 have been reported [11–13]. In a very compact instrument a mass resolution of 3500 has been achieved for ions traveling several times on oblique trajectories between two spatially extended sets of electrostatic fields defined by grids [14]. For compact TOFMS instruments with two oppositely mounted reflectrons in a multiple-ion-bounce mode a mass resolution in the range of 31,000–55,000 was achieved for biological molecules using up to 10 reflections [26]. For lighter molecules, a mass resolution of 18,000 after more than 100 reflections has been reported by Wollnik and Casares [15] and up to 50,000 after 31 reflections was achieved by Casares et al. [16] and Ishida et al. [17]. This approach requires pulsed reflectron voltages for the axial inlet and exit of the ions. Alternatively, cylindrical and toroidal electrostatic analyzers have been used to create a closed-orbit ion trajectory that is time focusing [27,28]. Ion packets inserted into this system can perform as many orbits as desired before directing the ion packets onto a detector. This approach also allows for high mass resolution, e.g., a mass resolution of 350,000 at mass-28 amu [28] and mass resolutions of 70,000 for biological samples with masses of 5000 amu have been achieved [29].

A survey of existing laboratory TOFMS instruments showed that no simple concept could be taken and transferred immediately into a design for an instrument suitable for space applications. Because of the physical constraints imposed by the spacecraft, such as stringent limitations on mass and power, as well as envelope volume and a maximum usable overall length of 1 m, the RTOF sensor was designed for three reflections using two ion mirrors.

2. The RTOF sensor and its reflectron

The reflectron time-of-flight (RTOF) mass spectrometer is part of the Rosetta orbiter spectrometer for ion and neutral analysis (ROSINA) instrument package, developed at the University of Bern, Switzerland, and onboard the Rosetta spacecraft on its way to comet Churyumov–Gerasimenko. The RTOF flight instrument and its performance are described in detail by Balsiger et al. [18].

The RTOF sensor allows the detection of cometary ions by injecting them into the sensor using an orthogonal extraction ion source. A storage ion source is used to ionize neutral cometary particles and inject into the sensor. The other elements of RTOF are the field-free drift tube, the reflectron, and the detector. Both ion sources use electron impact ionization to generate ions from neutral particles. The principal ion-optical elements of the sensor, using a multiple reflection configuration, are shown schematically in Fig. 1 and are described in detail by Scherer [19]. The final configuration of the RTOF flight sensor employs

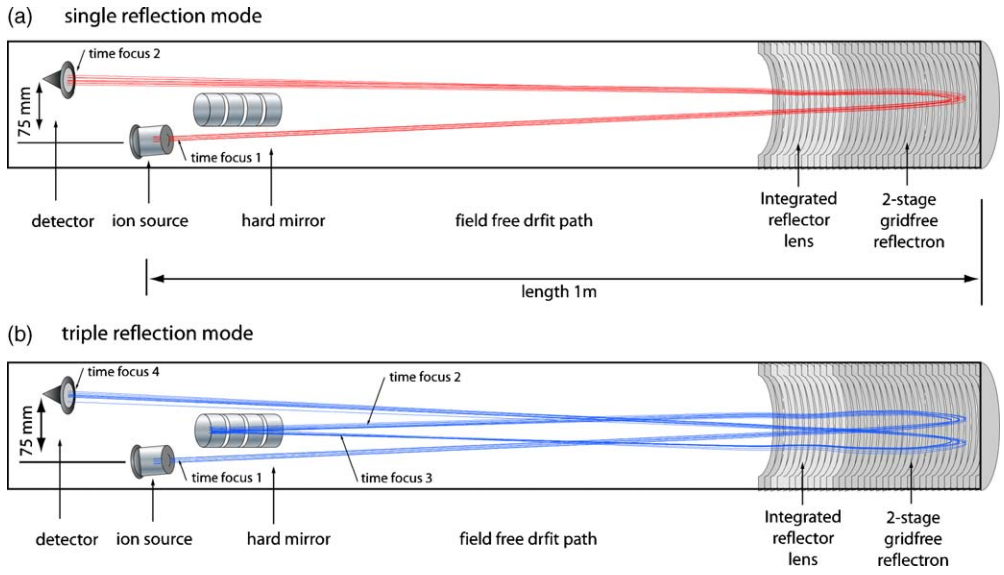

Fig. 1. Schematic of the ion optical elements of the RTOF sensor, its operation modes, and a few calculated ion trajectories. Panel (a) shows the single-reflection mode and panel (b) the triple-reflection mode. The two time foci for the single-reflection mode and the four time foci for the triple-reflection mode are indicated in the respective panels.

both types of ion sources, each with its own dedicated MCP detector [20], and shares the ion mirrors as well as the sensor structure. The two ion sources, with their corresponding detectors, are positioned orthogonally with respect to the cylindrical axis.

The reflectron for the RTOF sensor is a gridless design with the usual two individually adjustable stages; first a retarding region where the ions lose about two-thirds of their kinetic energy, and second the repelling region where the ions reverse their direction of motion. The RTOF sensor uses two different ion mirrors, which are positioned along the principal ion optical axis on opposite ends of the field-free drift path facing each other (Fig. 1). The ion optical symmetry axis is identical to the cylinder axis of the reflectron. The gridless reflectron, positioned at the end of the sensor opposite to the ion sources and detectors, includes a thick electrostatic lens at its front, the reflectron lens. The second reflectron is a much smaller ion mirror – called the hard mirror – that performs hard imaging of the ions, which means that the penetration depth of ions of different energies in the ion mirror are almost the same [21,22].

Having two ion mirrors in the system allows the operation of RTOF in a single- and a triple-reflection mode. In the single-reflection mode the ion trajectories start at an ion source, are reversed in the reflectron and end at the detector (Fig. 1a). In the triple-reflection mode the ions again start at the ion source and reverse their direction of motion in the reflectron, but are directed to the hard mirror. From the hard mirror, the ions are directed back to the reflectron and once again reverse their direction of motion in the reflectron before proceeding to the detector (Fig. 1b). In the triple-reflection mode the reflectron is used twice and the hard mirror is used once, effectively doubling the path length traveled in the same size instrument. Changing the voltage of the reflectron lens switches the instrument from one mode to the other. In triple-reflection mode the quality of the time focus is preserved, which leads to an increase of the mass resolution by a factor of almost two.

3. The reflectron

To cover a wide mass range, from hydrogen up to at least 300 atomic mass units (amu), simultaneously with having a high mass resolution, in a sensor of 1 m length, the only viable choice of instrument has been a reflectron TOFMS. The non-scanning operation of TOFMS provides the capability to cover the entire mass range in each measurement. In single-reflection mode RTOF covers the mass range from 1 to >500 amu [19]. Mass resolutions greater than 3000 at full width at half maximum (FWHM) have been achieved using multiple reflections, as has been described above, and are achieved with RTOF using the triple-reflection mode, which will be reported below. Therefore, the reflectron represents a key ion optical element of the RTOF sensor to meet the ambitious measurement requirements within the stringent resource constraints of a long-term space mission. The additional requirements for a space application made it necessary to come up with a completely novel reflectron design.

As discussed above, a gridless reflectron has obvious advantages over a conventional grid design. The electrical fields inside a gridless reflectron arise from the superposition of the individual potentials applied to the reflectron electrodes, and show considerable inhomogeneities. In addition, field inhomogeneities exist close to the electrodes resulting from their discrete nature. The treatment of inhomogeneous electrostatic fields in a gridless reflectron requires the aid of numerical methods to solve the Laplace equation, which was performed with the commercially available software tool SIMION 3D [23]. Both approaches – the ion optical simulations and the experimental verification – show for the gridless reflectron a similar electrical field as the

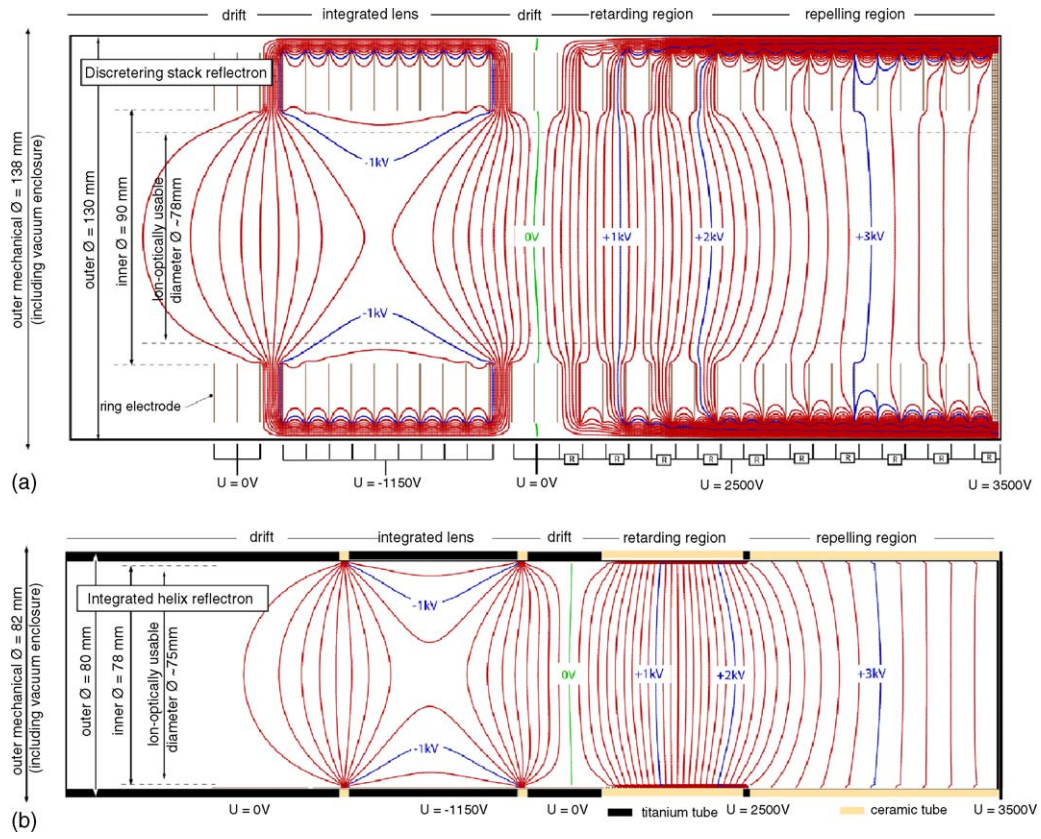

Fig. 2. Equipotential contours for the discrete ring stack reflectron (a) and for the integrated reflectron (b). Equipotential contours at 1 kV intervals are indicated in blue and the drift voltage, at ground potential, is marked in green. (For interpretation of the references to color in this figure legend, the reader is referred to the web version of the article.)

discrete two-stage ion mirror. These results correspond to the solution of Bergmann et al. [24], who expanded the potential in a series along the reflectron axis and solved it with the aid of spline functions.

The curved potential distribution in a gridless reflectron geometrically affects the trajectories of passing ions and therefore always exhibits geometrical focusing and defocusing properties. Due to the positive voltages in the reflectron with respect to the drift path, the reflectron entrance acts like the first half of a positive electrostatic Einzel lens, causing the ion beam to diverge when entering the reflectron.

In addition, a lens also influences the time-of-flight of an ion when different trajectories are taken. A positive (decelerating) lens affects the time of flight of ions more strongly than a negative lens does under similar focusing conditions because the longer off-axis trajectories are passed at lower ion energies. To minimize the positive lens effect of the reflectron, a thick negative lens, the reflectron lens, is used in front of the reflectron entrance in the RTOF sensor (see potential distribution given in Fig. 2), which performs all geometric focusing.

The reflectron lens allows us to geometrically alter the shape of the ion beam, as well as the main direction of the trajectories with regard to the optical axis. Adjusting the reflectron lens voltage allows manipulation of the inclination angle of the returning ion trajectories with respect to the optical axis of the system. Because of this feature we can omit two sets of deflector plates and their associated power supplies at the exit of the ion source to manipulate the direction of propagation of the ion beam. The practical application of this feature is demonstrated for the two different operating modes of the RTOF sensor (see Fig. 1). A larger negative voltage applied to the reflectron lens will further deflect the ion trajectories, switching the RTOF operation from single-reflection to triple-reflection mode. For the single-reflection mode the reflectron lens voltage is in the range −3200 to −2500 V below the drift potential, and for the triple-reflection mode the voltage is between −4000 and −3700 V below the drift potential.

The first laboratory model of a gridless reflectron for the RTOF sensor was a stack of 33 ring electrodes, made of stainless steel, with an inner diameter of 90 mm, an outer diameter of 130 mm, and spaced equidistantly with a distance of 7 mm. The entrance, the reflectron lens, consisted of a series of 11 electrodes at the same potential, followed by 10 individually adjustable sets of two consecutive ring electrodes used to generate the retarding and repelling electrostatic fields. The ion optical performance of the RTOF sensor was optimized and a set of voltages for these 10 sets of ring electrodes was found. Simulations with SIMION for the optimized experimental voltages showed an electrical potential configuration along the reflectron similar to that of a discrete two-stage reflectron. The necessity to reduce the large number of individually adjustable reflectron potentials led to a solution with only three adjustable reflectron voltages; the drift

voltage, the retarding voltage, and the repelling voltage. This change had no affect on the performance of the RTOF sensor. The individual ring electrodes of the reflectron were connected by a high-impedance resistor chain with an adjustable middle electrode, at retarding voltage, to realize the required potential distribution for the second-order time-focusing condition. The successful operation of a gridless two-stage reflectron has been demonstrated with the ring stack configuration using three independent voltages.

For space applications the RTOF sensor needed a vacuum enclosure, and severe mass and volume constraints were imposed on the design. The vacuum enclosure is needed because the RTOF sensor is launched under UHV conditions for contamination and cleanliness reasons. The implementation of all these requirements led to the novel design of a two-stage gridless reflectron, the so-called integrated reflectron. The basic idea was to combine the ion optical functions, the potential divider, the vacuum enclosure, and the feed-throughs into one integral unit.

The voltages, and thus the electrical fields inside the reflectron, are defined by a voltage drop over a resistive coating in the form of a helix applied to the inner surface of a ceramic tube with an inner diameter of 78 mm. The total resistance over the entire helix is about 1.5 GΩ. The total resistance value is determined for a maximum ion current of about 1 nA extracted from the ion source and dumped onto the resistive coating without changing the reflectron voltages more than 1 V. The high impedance of the reflectron minimizes the power consumption for the reflectron high-voltage power supplies. For typical operation voltages in the kV range the power consumption stays in the mW range, which is important for a space application.

The potential drop is constant along the helix and matches exactly the helix pitch. Therefore, the integrated reflectron shows an exact linear potential variation along the cylindrical boundary of the integrated reflectron. In addition, the helix minimizes electrical fringe fields close to the cylindrical boundary of the reflectron structure, a significant improvement over a ring stack reflectron made out of discrete electrode rings. Fig. 2 shows the ion-optical simulation of the equipotential contour lines for the discrete ring stack reflectron (Fig. 2a) and for the integrated reflectron (Fig. 2b). The two-stage electric field gradients are the same for both types of reflectrons aside from the field perturbations close to the ring electrodes in the conventional design. A nearly perfect potential distribution for a gridless reflectron is thus generated in the entire inner volume of the unit.

The resistor helix consists of two segments, where the length of the retarding field is half that of the repelling field but the potential drop over the retarding region is twice the value of the repelling region, according to the second-order focus condition derived for the conventional two-stage reflectron. Fig. 3 shows an engineering drawing of the final design of the gridless integrated reflectron complete with the reflectron lens at the entrance and the retarding and repelling electrodes with the helical path on the inside.

We developed a special procedure to paint the resistor helix with a computerized, numerically controlled paint dispenser at the inner surface of the ceramic tube, which is then subjected to a sintering process. The two helix segments are brazed together with a metallic ring electrode in between. The backplane at the end of the reflection section consists of a planar solid disc made out of titanium. Fig. 4 shows a photograph of the retarding and repelling region of the integrated reflectron with the ceramic tube elements and the brazed titanium electrode. This design makes it possible to apply the reflectron voltages to the resistor helix terminals from the outside, acting as a high-voltage feed-through and eliminating the need for dedicated high-voltage feed-throughs to apply the reflectron potentials.

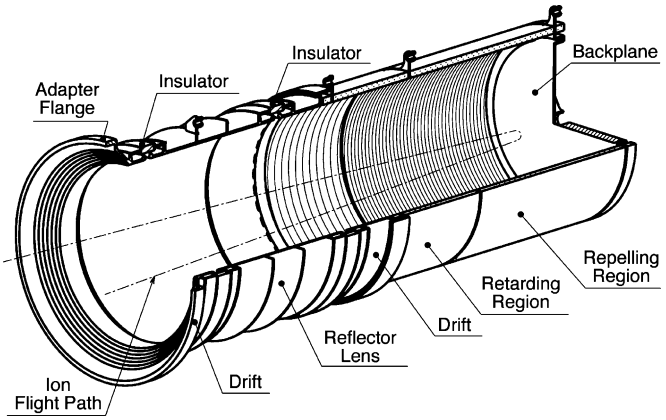

Fig. 3. Engineering drawing of the individual segments of the integrated reflectron. The elements are the reflectron lens in the entrance area, an intermediate electrode at drift potential, two following segments with a resistive helix applied to the inner surface of a ceramic tube, which generate the retarding and repelling electrostatic fields, and a metallic backplane at the end.

The ceramic structure of the integrated reflectron simultaneously acts as the ultra-high-vacuum enclosure for the RTOF sensor and is an integral part of the overall sensor structure. The ratio of the inner, ion optically usable diameter and outer tube diameter, including the vacuum housing, is maximized, resulting

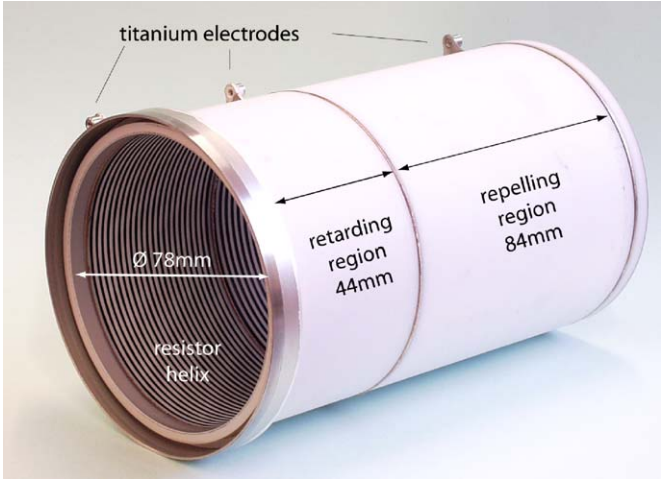

Fig. 4. Photograph presents an exterior view of the retarding and repelling regions of the integrated reflectron. The electrical contact is made from the outside at the titanium electrodes brazed vacuum-tight between the ceramic tubes. The backplane is a solid titanium plate where the repelling potential of the reflectron is applied. The electrodes between the repelling and the retarding region and the entrance electrode are titanium rings. The assembly of drift tube and reflectron lens is welded to the front flange of the retarding region.

in a more than 50% weight reduction compared to a classic ring stack reflectron that requires an additional vacuum housing.

The technology to fabricate ultra-high-vacuum brazing connections between the ceramic tubes and the titanium electrodes was developed at the Swiss Federal Laboratories for Materials Testing and Research (EMPA) [25] in Dübendorf, Switzerland, which performed the manufacturing and processing of the integrated reflectron. The integrated reflectron was subjected to a vacuum-keeping test at the EMPA laboratories. Following thermal conditioning, the pump valve was closed and the vacuum pressure inside the integrated reflectron stayed in the high 10^{-8} mbar range for more than a week. Actually, the titanium elements of the integrated reflectron acted as an active getter surface and the pressure inside the integrated reflectron even decreased further with time. Successfully passing the vacuum-keeping test was a critical milestone in the RTOF development, since the sensor had to be launched into space evacuated to UHV levels to avoid contamination by atmospheric gases or rocket propellants.

The approach of applying a continuous resistor coating over the entire inner surface of the ceramic tube was investigated in the course of the design process, but the experimental processing results showed that the homogeneity of the applied resistor coating, and subsequently the homogeneity of the electric field, could not be achieved with this method. Resistively coated glass tubes with sufficient homogeneity only recently became commercially available from Burle Industries, Inc., and might be a future alternative to the design presented here when tubes with a sufficiently large inner diameter become available. Additional research is required on these glass tubes to develop and verify the proper brazing process to provide the vacuum-tight connection and to proof the reliability with regard to vibration levels to be encountered during a rocket launch.

4. Results

The performance of the RTOF laboratory prototype using the integrated reflectron is evaluated with regard to the ability to

Table 1
The accuracy δm_i of the mass determination for a sample mixture of noble gases and a mass triplet at mass-28 amu is tabulated for three different calibration methods

Species	Mass, m_{tab} (amu)	Case I		Case II		Case III		TOF (μs)	ΔT (ns)	$m/\Delta m$, FWHM
		m_i (amu)	δm_i (ppm)	m_i (amu)	δm_i (ppm)	m_i (amu)	δm_i (ppm)			
$^{1}H_2^+$	2.015101	2.014973	−64	2.014963	−68	2.014803	−148	8.5195	1.2	3416
$^{4}He^+$	4.002055	4.002055	0	4.002055	0	4.001850	−51	11.9800	1.6	3695
$^{12}C^+$	11.999451	11.999363	−7	11.999420	−3	11.999154	−25	20.6965	2.5	4110
$^{12}C^{1}H^+$	13.007276	13.007491	17	13.007556	21	13.007288	1	21.5457	2.2	4822
$^{12}C_2{}^{1}H_3{}^{++}$	13.511189	13.511616	32	13.511684	37	13.511416	17	21.9580	2.2	4990
$^{12}C^{16}O^{++}$	13.996909	13.997294	28	13.997366	33	13.997098	13	22.3480	2.2	5079
$^{14}N^+$	14.002525	14.002767	17	14.002840	22	14.002571	3	22.3524	2.7	4182
$^{12}C^{1}H_2{}^+$	14.015101	14.015517	30	14.015589	35	14.015320	16	22.3625	2.6	4235
$^{16}O^+$	15.994366	15.994188	−11	15.994276	−6	15.994007	−22	23.8845	2.8	4236
$^{12}C^{1}H_4{}^+$	16.030751	16.031140	24	16.031229	30	16.030960	13	23.9120	2.7	4394
$^{1}H_2{}^{16}O^+$	18.010016	18.009858	−9	18.009963	−3	18.009696	−18	25.3409	2.4	5333
$^{40}Ar^{++}$	19.980917	19.981049	7	19.981171	13	19.980907	0	26.6882	2.7	4975
$^{20}Ne^+$	19.991892	19.992068	9	19.992190	15	19.991926	2	26.6956	2.8	4769
$^{12}C_3{}^{1}H_4{}^{++}$	20.015101	20.014415	−34	20.014538	−28	20.014274	−41	26.7104	2.5	5342
$^{12}C_2{}^{1}H_3{}^+$	27.022926	27.023136	8	27.023320	15	27.023080	6	31.0263	2.9	5316
$^{12}C^{16}O^+$	27.994366	27.995658	46	27.995851	53	27.995615	45	31.5785	3.6	4393
$^{14}N_2{}^+$	28.005599	28.006319	26	28.006512	33	28.006276	24	31.5845	3.3	4810
$^{12}C_2{}^{1}H_4{}^+$	28.030751	28.031204	16	28.031397	23	28.031161	15	31.5985	3.3	4818
$^{13}C^{16}O^+$	28.997721	29.000198	85	29.000400	92	29.000218	86	32.1389	3.3	4870
$^{15}N^{14}N^+$	29.003634	29.006166	87	29.006368	94	29.006186	88	32.1422	3.3	4870
$^{12}C_2{}^{1}H_5{}^+$	29.038576	29.034675	−134	29.034878	−127	29.034696	−134	32.1422	3.3	4872
$^{16}O_2{}^+$	31.989281	31.989634	11	31.989863	18	31.989647	11	33.7515	3.6	4698
$^{40}Ar^+$	39.961835	39.961256	−14	39.961560	−7	39.961392	−11	37.7155	3.8	4902
$^{12}C^{12}O_2{}^+$	43.989281	43.989281	0	43.989622	8	43.989482	5	39.5675	4.5	4370
$^{82}Kr^+$	81.912936	81.913346	5	81.914055	14	81.915071	26	53.9699	5.7	4734
$^{83}Kr^+$	82.913587	82.912497	−13	82.913215	−4	82.914252	8	54.2977	5.6	4848
$^{84}Kr^+$	83.910958	83.910230	−9	83.910958	0	83.912014	13	54.6230	5.5	4927
$^{86}Kr^+$	85.910062	85.910244	2	85.910992	11	85.912088	24	55.2694	5.2	5314
$^{129}Xe^+$	128.904231	128.900603	−28	128.901783	−19	128.903765	−4	67.6855	7.5	4514
$^{131}Xe^+$	130.904533	130.893402	−85	130.894601	−76	130.896626	−60	68.2062	8.0	4263
$^{132}Xe^+$	131.903606	131.901126	−19	131.902335	−10	131.904381	6	68.4680	6.0	5680
$^{134}Xe^+$	133.904846	133.902635	−17	133.903865	−7	133.905954	8	68.9850	7.1	4858
$^{136}Xe^+$	135.906671	135.904145	−19	135.905395	−9	135.907526	6	69.4982	6.8	5110
Mean			28		28		30			

Case I uses a quadratic calibration based on the two mass ^{4}He and $^{12}C^{16}O_2$. Case II shows a mass calibration based on the two mass lines ^{4}He and ^{84}Kr. Case III uses a multi-mass fit. The last row contains the mean for the deviation in each case. The last three columns indicate the time-of-flight (TOF), the time spread (ΔT), and the mass resolution at FWHM in the triple-reflection mode.

determine an absolute mass calibration as well as the achievable mass resolution. The mass calibration for a time-of-flight mass spectrometer is established by the simple equation:

$$m = \left(\frac{t - t_0}{C}\right)^2 \tag{1}$$

Eq. (1) relates the measured flight time t and the mass m of an ion. The constant C and the time offset t_0 can easily be determined by identifying two known masses, m_1 and m_2, at their time-of-flight t_1 and t_2 in the TOF spectrum by

$$C = \frac{t_1 - t_2}{\sqrt{m_1} - \sqrt{m_2}} \tag{2}$$

and

$$t_0 = \frac{\sqrt{m_2}t_1 - \sqrt{m_1}t_2}{\sqrt{m_2} - \sqrt{m_1}} \tag{3}$$

The correctness of the identification of the two mass lines, and of the mass calibration, can easily be verified because all mass peaks in the resulting mass spectrum have to be located at integer mass numbers (to first order). Sometimes the accuracy of the mass scale can be improved by using more than two reference masses. For N reference mass lines the constants C and the time offset t_0 for the mass calibration (Eq. (1)) can be calculated by

$$C = \frac{N\sum_{i=1}^{N} t_i^2 - \left(\sum_{i=1}^{N} t_i\right)^2}{N\sum_{i=1}^{N}\left(\sqrt{m_i}t_i\right) - \sum_{i=1}^{N}\sqrt{m_i}\sum_{i=1}^{N} t_i} \tag{4}$$

and

$$t_0 = \frac{\sum_{i=1}^{N}\left(\sqrt{m_i}t_i\right)\sum_{i=1}^{N} t_i - \sum_{i=1}^{N}\sqrt{m_i}\sum_{i=1}^{N} t_i^2}{N\sum_{i=1}^{N}\left(\sqrt{m_i}t_i\right) - \sum_{i=1}^{N}\sqrt{m_i}\sum_{i=1}^{N} t_i} \tag{5}$$

In Table 1 the deviation δm_i of the mass calibration from the tabulated mass values for a sample mixture of noble gases (He, Ne, Ar, Kr, and Xe) and a mass triplet at mass-28 amu (C_2H_4, CO, and N_2) is computed for three different calibration methods. The deviation δm_i is determined as

$$\delta m_i = \frac{m_i - m_{\text{tab}}}{m_{\text{tab}}} \tag{6}$$

where m_i is the computed mass (using a certain mass calibration method) and m_{tab} is the tabulated mass. In this measurement the mass range from hydrogen to xenon has been covered and 33 mass lines of sufficient intensity have been selected for detailed analysis. Case I uses a quadratic calibration according to Eq. (1) based on two references mass lines at ^{4}He and $^{12}C^{16}O_2$. A mean value of the accuracy for the mass determination of 28 ppm has been achieved over the considered mass range (see case I in Table 1). Case II shows a mass calibration based on two reference mass lines, ^{4}He and ^{84}Kr. A mean value of the accuracy for the mass determination of 28 ppm has been achieved over the entire mass range (see case II in Table 1). Finally, in method III, a multi-mass fit has been calculated using 33 intense mass lines (see case III in Table 1). Here, we achieve a mean value for the accuracy of the mass determination of 30 ppm. The mass accuracy is best for case I, but only slightly worse for the other cases. Statistically speaking, these deviations are not sufficient to strongly favor one method over another. However, the simplicity of using only two reference masses makes us prefer this method. No additional information is gained using the multi-mass fit of case III. The mass accuracies are about a factor of 10 better than the mass resolution (see below), and are limited by the finite resolution of the digitizing electronics (0.5 ns sampling intervals). Further improvements in mass accuracy are expected when using shorter sampling intervals.

In addition, Table 1 lists the time-of-flight (TOF), the time spread (ΔT) at FWHM, and the corresponding mass resolution at FWHM. The mass resolution versus mass is plotted in Fig. 5, with the theoretical mass resolution function fitted to the measured data. The typical time-of-flight (TOF) ranges from 8.5 μs for hydrogen up to 68 μs for the xenon isotopes in the triple-reflection mode. The measured time spread is 1.25 ns FWHM for hydrogen and about 6 ns for the xenon isotopes, corresponding to a mass resolution well above 3000 at FWHM in the low mass range and up to 5000 in the high mass range (see Fig. 5).

Fig. 6 shows details of the mass spectrum for three interesting mass triplets at mass-14 amu (Fig. 6a), mass-28 amu (Fig. 6b), and mass-29 amu (Fig. 6c). The triplet at mass-14 amu is composed of doubly charged CO, singly charged atomic N, and singly charged CH_2. The mass triplet at mass-28 amu is composed of the singly charged molecules CO, N_2, and C_2H_4, which are clearly distinguished even at the 10% peak height. In Fig. 6c, the triplet at mass-29 amu is shown where the isotopic $^{14}N^{15}N/^{13}C^{16}O$ peak is separated from the C_2H_5 peak below the 1% level. The components of the $^{14}N^{15}N/^{13}C^{16}O$ peak are not resolved and therefore indicated by a fitted Gaussian curve for each component.

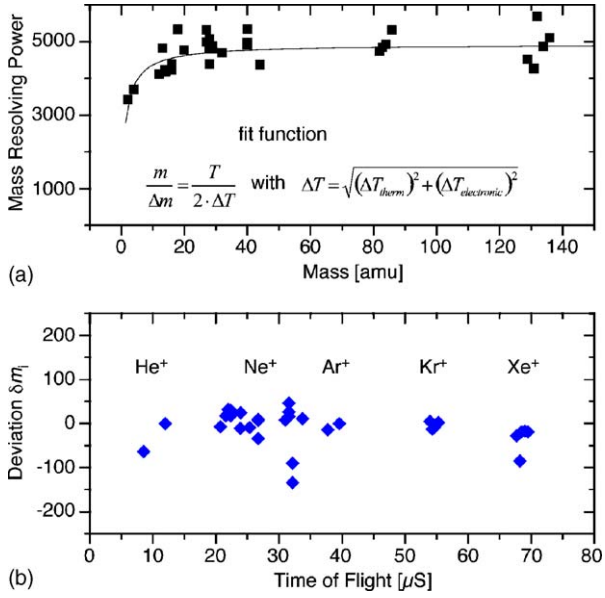

Fig. 5. (a) Mass resolving power vs. mass, including the theoretical resolution fitted into the data points, taking into account the thermal energy of the ions as well as a contribution by the electronics. (b) The deviation δm_i vs. the time-of-flight, with regard to the deviation in the mass calibration as shown for case I using the two calibration masses He and CO_2. The mean value of the deviation is around 28 ppm (see Table 1).

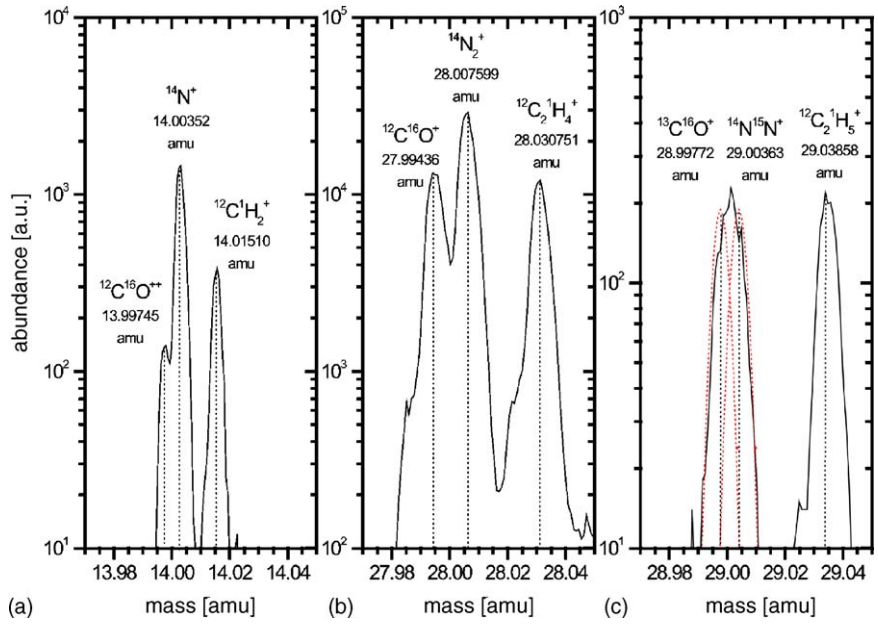

Fig. 6. Sections of the spectrum at the mass triplets at mass-14 amu, mass-28 amu, and mass-29 amu. Panel (a) illustrates the mass resolution at mass-14 amu with regard to the doubly charged CO molecule, singly charged atomic N atom, and singly charged CH_2 molecule. Panel (b) presents the mass triplet at mass-28 amu with CO, N_2, and C_2H_4 molecules. Panel (c) shows the mass triplet at mass-29 amu. The isotopes of $^{13}C^{16}O$ and $^{14}N^{15}N$ are not resolved and shown as Gaussian fitted curves, whereas the peak of $^{12}C_2{}^1H_5$ is clearly separated from the isotopic peak.

5. Conclusion

The integrated reflectron is a compact, gridless ion mirror based on a ceramic structure, which also serves as the ultra-high-vacuum enclosure for the sensor housing. Compared to the classical ring stack reflectron, which needs an additional vacuum enclosure, our design results in a 50% mass savings by maximizing the ratio of the ion optical usable inner diameter (78 mm) with respect to the overall outer diameter (80 mm). The generation of the retarding and repelling electrical fields along the resistor helix applied to the inner surface of the ceramic reflectron tube negates the fringe fields at the cylindrical boundary of the reflectron structure, and an optimized homogeneity of the electrostatic field is achieved. The electrostatic lens at the entrance of the reflectron (the reflectron lens) performs all the necessary geometric focusing and allows switching between the single- and triple-reflection mode, thus, removing the need for two pairs of deflection plates. The integrated reflectron successfully demonstrated the feasibility of a construction combining ceramic structures with metallic electrodes. This technique has been adapted for all ion optical elements in the RTOF flight sensor, including the ion sources. This design made it possible to meet the stringent mass constraints for the RTOF flight sensor. The integrated reflectron design presented in this paper constituted the basis for the final RTOF flight sensor design.

Acknowledgments

Financial support from the Swiss National Science Foundation and the ESA PRODEX program is gratefully acknowledged. The joining technology of the integrated reflectron was made possible by EMPA Swiss Federal Laboratories for Material Testing and Research, Dübendorf, Switzerland, with a particular contribution of B. Zigerlig and H.R. Elsener. The authors gratefully acknowledge the contributions in manufacturing of the laboratory instrument under the direction of H. Hofstetter at the University of Bern.

References

[1] W.C. Wiley, I.H. McLaren, Rev. Sci. Instrum. 26 (1955) 1150.
[2] V.I. Karataev, B.A. Mamyrin, D.V. Shmikk, Sov. Phys. JETP 16 (1972) 1177.
[3] B.A. Mamyrin, V.I. Karataev, D.V. Shmikk, V.A. Zagulin, Sov. Phys. JETP 37 (1973) 45.
[4] P. Wurz, Ph.D. Thesis, Technische-Naturwissenschaftliche Fakultät, Technische Universität Wien, Austria, 1990.
[5] T. Bergmann, T.P. Martin, H. Schaber, Rev. Sci. Instrum. 60 (1989) 792.
[6] K. Walter, T. Boesl, W. Schlag, Int. J. Mass Spectrom. Ion Process. 71 (1986) 309.
[7] R. Grix, R. Kutscher, G. Li, U. Grüner, H. Wollnik, Rapid Commun. Mass Spectrom. 2 (1988) 83.
[8] R. Kutscher, R. Grix, G. Li, H. Wollnik, Int. J. Mass Spectrom. Ion Process. 103 (1991) 117.
[9] H. Wollnik, Int. J. Mass Spectrom. Ion Process. 131 (1994) 387.
[10] T. Bergmann, T.P. Martin, H. Schaber, Rev. Sci. Instrum. 61 (1990) 2592.
[11] D.J. Beussmann, P.R. Vlasak, R.D. McLane, M.A. Seeterlin, C.G. Enke, Anal. Chem. 67 (1995) 3952.
[12] T.J. Cornish, R.J. Cotter, Anal. Chem. 65 (1993) 1043.
[13] H. Wollnik, M. Przewlowka, Int. J. Mass Spectrom. Ion Process. 96 (1989) 267.
[14] C.-S. Su, D.J. Beussmann, Int. J. Mass Spectrom. Ion Process. 88 (1989) 21.
[15] H. Wollnik, A. Casares, Int. J. Mass Spectrom. Ion Process. 227 (2003) 217.

[16] A. Casares, A. Kholomeev, H. Wollnik, Int. J. Mass Spectrom. Ion Process. 206 (2001) 267.
[17] Y. Ishida, M. Wada, Y. Matsuo, I. Tanihata, A. Casares, H. Wollnik, Nucl. Instrum. Meth. B 219–220 (2004) 468.
[18] H. Balsiger, K. Altwegg, E. Arijs, J.-L. Bertaux, J.-J. Berthelier, B. Block, P. Bochsler, G.R. Carignan, L. Duvet, P. Eberhardt, B. Fiethe, J. Fischer, L.A. Fisk, S.A. Fuselier, A.G. Ghielmetti, F. Gliem, T.I. Gombosi, M. Illiano, T. Koch, E. Kopp, A. Korth, K. Lange, H. Lauche, S. Livi, A. Loose, T. Magoncelli, C. Mazelle, M. Mildner, E. Neefs, D. Nevejans, H. Rème, J.A. Sauvaud, S. Scherer, A. Schoenemann, E.G. Shelley, J.H. Waite, C. Westermann, B. Wilken, J. Woch, H. Wollnik, P. Wurz, D.T. Young, ESA SP-1165, in press.
[19] S. Scherer, Ph.D. Thesis, Space Research and Planetary Sciences, University of Bern, Switzerland, 1999.
[20] R. Schletti, P. Wurz, S. Scherer, Rev. Sci. Instrum. 72 (2001) 1634.
[21] M. Hohl, P. Wurz, S. Scherer, K. Altwegg, H. Balsiger, Int. J. Mass Spectrom. Ion Process. 188 (1999) 189.
[22] M. Hohl, Master's Thesis, Space Research and Planetary Sciences, University of Bern, Switzerland, 1998.
[23] SIMION 3D, Revision 6.0.
[24] T. Bergmann, H. Groehlich, G. Malegiannakis, T.P. Martin, H. Schaber, Rev. Sci. Instrum. 61 (1989) 2585.
[25] B. Zigerlig, Technical Report UMIACS-TR-95-12 and CS-TR-3408, 1998.
[26] C.K.G. Piyadasa, P. Håkansson, T.R. Ariyaratne, Rapid Commun. Mass Spectrom. 13 (1999) 620.
[27] M. Toyoda, D. Okumura, M. Ishihara, I. Katakuse, Int. J. Mass Spectrom. 38 (2003) 1125.
[28] D. Okumura, M. Toyoda, M. Ishihara, I. Katakuse, Nucl. Instrum. Meth. A 519 (2004) 331.
[29] M. Ishihara, M. Toyoda, I. Katakuse, Proceedings of the Fifth International Symposium on Atomic Level Characterizations for new Materials and Devices, in press.